EPR investigation of pure and Co-doped ZnO oriented nanocrystals.

— Source link ↗

Adrien Savoyant, Hatim Alnoor, Sylvain Bertaina, Omer Nur ...+1 more authors

Institutions: Aix-Marseille University

Related papers:

- Structural, optical, and magnetic properties of Co-doped ZnO nanorods fabricated by a facile solution route

- Synthesis of Nanocrystalline Co Doped ZnO by Chemical Route and Its Magnetic Properties

- Enhancement of room-temperature ferromagnetism and dielectric response in nanocrystalline ZnO co-doped with Co and Cu

- Effect of low Co-doping on structural, optical, and magnetic performance of ZnO nanoparticles

- Physical and magnetic properties of (Co, Ag) doped ZnO nanoparticles

EPR investigation of pure and Co-doped ZnO oriented nanocrystals

Adrien Savoyant, H Alnoor, Sylvain Bertaina, O Nur, M Willander

EPR investigation of pure and Co-doped ZnO oriented nanocrystals

A. Savoyant,[1] H. Alnoor,[2] S. Bertaina,[1] O. Nur,[2] and M. Willander[2]

[1]IM2NP, CNRS UMR 6242, FST, Aix-Marseille Université, F-13397 Marseille Cedex 20, France
[2]Department of Science and Technology (ITN),
Linköping University, SE-601 74 Norrköping, Sweden

Pure and cobalt-doped zinc oxide aligned nanorods have been grown by the low-temperature (90 °C) aqueous chemical method on amorphous ZnO seed layer, deposited on a sapphire substrate. High crystallinity of these objects is demonstrated by the electron paramagnetic resonance investigation at liquid helium temperature. The successful incorporation of Co^{2+} ions in substitution of Zn^{2+} ones in the ZnO matrix has also been confirmed. A drastic reduction of intrinsic ZnO nanorods core defects is observed in the Co-doped samples, which enhances the structural quality of the NRs. The quantification of substitutional Co^{2+} ions in the ZnO matrix is achieved by comparison with a reference sample. The findings in this study indicate the potential of using the low-temperature aqueous chemical approach for synthesizing material for spintronics applications.

I. INTRODUCTION

The physics of nanocrystals is a wide area of research, which is particularly concerned with nanoelectronics. In this context, nanosized crystals are employed to obtain augmented efficiency, small size, low cost, and special physics of confinement[1–3]. Compared to ultra-thin films (2D) and dots (0D), one-dimensional (1D) nanostructures present the advantage to combine both high surface area/volume ratio and orientability, but also an intrinsic sensitivity to mechanical stress. This last point is of particular importance for polar crystals, in which surface effects and/or deformation can induce some very strong internal electric fields (nano-piezoelectricity). An example of such a system is given by ZnO nanorods (NRs). Combined or not with other materials (e.g ZnO-NRs/GaN), they are in use in many functional electronic devices, including fast UV detectors, pressure sensors[4], and light-emitting diode[5–9]. These ZnO NRs can be doped with a wide variety of elements[5–8,10–12], mainly performed with the aim of tunning the semiconducting properties (e.g band gap).

The possibility for doping ZnO NRs with magnetic impurities offers a way to add magnetic properties to these nanostructured material to develop spintronics and magneto-optical devices. The main candidates to bear localized high spin in ZnO are Mn^{2+} ($S = 5/2$) and Co^{2+} ($S = 3/2$) ions, in substitution of the Zn^{2+} ions at relatively low concentration. Such diluted magnetic semiconductors (DMS) have been widely studied for the bulk and thin films materials[13–21]. They are paramagnetic at all temperatures and present different spin properties: slow relaxation and low (easy-axis) anisotropy for Mn^{2+}, fast relaxation and high (easy-plane) anisotropy for Co^{2+}, both properties which are related to the spin-lattice coupling. In practice, even the magnetic anisotropy of Co^{2+} in ZnO is far too weak ($\sim$ 4 K) to influence some properties of interest at room temperature. To date, devices involving the magnetic properties of bulk ZnO-based DMS are considered at the stage of research and development.

Nevertheless, the situation can be different for NRs, where the induced or intrinsic electric fields may be strong enough to modify this magnetic anisotropy, which actually depends on spin-orbit coupling and crystal field. Compared to other DMS, ZnO:Co is the more likely to demonstrate this magneto-electrical coupling, because the Co^{2+} high-spin ground state ($^4A_2$) is not fully symmetric: effective **L.S** interaction is intense, and so is the spin-lattice coupling. The odd-order components of the internal electric field multipole developement can couple the ground state to excited configurations, while even components can modify the crystal-field, thus indirectly tunning the magnetic anisotropy. For these reasons, the detailed knowledge of the ground state of substitutional Co^{2+} ions in ZnO 1D nanostructures is a matter of great interest.

Among several probing experiments, electron paramagnetic resonance (EPR) offers a unique way to investigate ground states of localized magnetic impurities in the NRs and, in turn, to deduce many structural, electronic and magnetic information on these impurities and the NRs themselves. In EPR spectrometry of DMS, not only the magnetic impurities concentration (x) matters, but also the absolute number (N) of them: low x and high N are simultaneously required, in order to lower the line width and to increase the signal intensity. Detecting low concentration of spin in DMS nanocrystals then implies the need to deal with a large collection of

such objects, each one contributing to the EPR signal. When it is detected, the EPR signal can give precious information on the magnetic impurities and their direct environment at the atomic scale. If the nanocrystals are single crystalline in nature and possess a coherent orientation, the obtained information is maximal.

In this paper, we report on EPR study on high crystalline and well-aligned pure and cobalt-doped ZnO NRs, performed at liquid helium temperature. The EPR lines are just above the limit of detection and give precious information on the ZnO NRs structure at the atomic scale. We find that pures NRs contains no other detectable magnetic impurities than a well-known core defect at $g \sim 1.96$. The subsequent incorporation of Co^{2+} ions reveals a very high crystallinity of the NRs, comparable to those of bulk and single microcrystal. Interestingly, we find that this addition of cobalt drastically reduces the number of the core defects detected in the pure NRs. The observed axial anisotropy of the Co-related EPR lines indicates that all the NRs containing cobalt are well-aligned together, within a dispersion of less than few degrees. The absolute quantities of the substitutional Co^{2+} ions are determined by comparison with a reference sample.

II. METHODS

The pure and Co-doped ZnO NRs were synthesized via the low-temperature aqueous chemical method, on a double side polished sapphire substrates (3mm×3mm×0.43mm). A seed layer consisting of ZnO nanoparticles (20-50 nm diameter) was spin coated on the sapphire substrates. This coating was repeated four times to obtain uniform spatial distribution of the nanoparticles. This step was followed by annealing in a conventional oven at 120 °C for 10 minutes.
For the synthesis of the Co-doped ZnO NRs, a 0.075 M concentration of hexamethylenetetramine (HMTA) was prepared separately in deionized (DI) water and stirred for one hour at room temperature. Then, diluted solutions of Cobalt(II) acetate tetrahydrate with different atomic concentration (0%, 2% and 5%) were mixed with the HMTA solution and stirred for 15 hours. After that, a 0.075 M prepared concentration of zinc nitrate hexahydrate was added dropwise to the three above mixed solutions and stirred for three hours. Finally, the seed layer coated sapphire substrates were submerged vertically inside the synthesis solutions and kept in a preheated oven at 90 °C for 6 hours. After the NRs growth, the three samples were rinsed with DI water to remove any residuals, and finally dried using

blowing nitrogen.
We thus obtained three NRs samples, S0, S1, and S2 (schematized in Fig. 1), which differ in the cobalt atomic concentration of the $Co(C_2H_3O_2)_2 \cdot 4$ H_2O synthesis solution, respectively 0%, 2%, and 5%. These three samples contain approximately 1.4×10^7, 1.9×10^7 and 10^7 NRs per mm^2, respectievly. They have a common length of 3.5 μm, and mean diameters of 220, 210, and 300 nm, respectively. Scanning electron microscopy (SEM) imaging (Fig. 1) show mostly aligned NRs in each of the three samples.
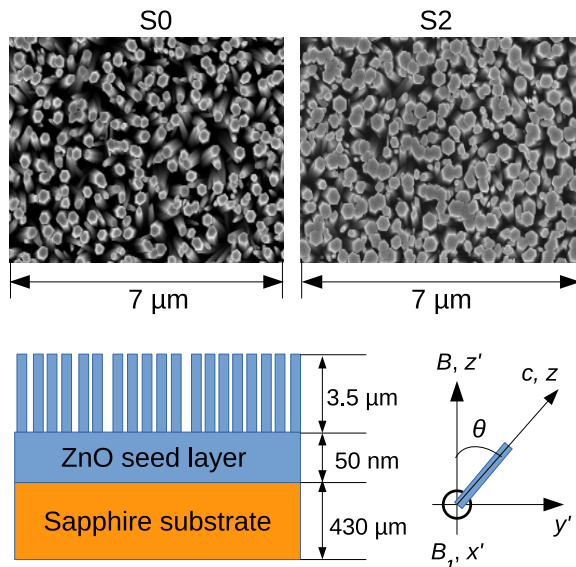

Figure 1: (color online) Top: SEM imaging of pure (S0) and cobalt-doped (S2) NRs. Bottom: schematic of the NRs samples and definition of the angle θ between the magnetic field B and the c-axis of the NRs. Microwave magnetic field B_1 is perpendicular to both B and c.

EPR measurements have been performed on a conventional Bruker EMX continuous wave spectrometer operating at X-band ($\nu = 9.62$ GHz) using a standard TE_{102} mode cavity. The samples were glued on a quartz suprazil rod using a small amount of vacuum grease. The orientation of the samples was insured by an automatic goniometer with a precision of .25°. Due to the low Co concentration, saturation recovery measurements have been performed and microwave power has been chosen to avoid signal saturation. The modulation of the static field (5 and 1 G) at a frequency of 100kHz was used with a lock in amplifier to increase sensitivity and record the derivative of the EPR signal. The measurements have been performed at a temperature between 5 K and 17 K. Above 17 K, the signal was too weak and too broad, due to relaxation processes.
For spin quantification, we have performed the same experiment on a ZnO thin film (TF)

doped with 0.5 % of cobalt grown by molecular beam epitaxy (MBE), and of similar dimension (3mm×3mm×1.3μm). Assuming a homogeneous doping, this reference sample contains approximatively 2.5×10^{15} Co ions (2 Zn sites per elementary cell of volume 48 Å^3).

III. RESULTS

A. Pure nanorods

We first study pure ZnO NRs and compare the EPR spectra at various steps of their fabrication. Being sensitive to extremely small energy splittings, EPR can detect some very little amount of undesired impurities or defects. It is then useful to examine separately the EPR signal of each part of the final object, in order to accurately detect pollution and to identify signals arising from nanocrystals.

In the figure 2-a, the EPR spectrum of the quartz sample holder (SH) used in all measurements is shown. It displays two lines, large and narrow, just above the noise, and arising from a very little quantity of isotropic magnetic defects within the amorphous quartz. These signals are almost identically present in all other spectra performed with the same experimental conditions (MW power, temperature, modulation, etc.).
Fig. 2-b shows that none detectable defects are present in the sapphire substrate used in all samples. When adding the nanometric ZnO seed layer (Fig. 2-c), no additional signals are detected. The intensity's variability of the narrow SH line may be attributed to some slight differences of the SH position within the cavity, and to its very low signal/noise ratio.

The EPR spectra of pure NRs grown on the ZnO seed layer is shown on figure 2-d. It displays, in addition to the SH signals, a big sharp line at 350 mT ($g \simeq 1.96$), apparently structured. This is a well-know defect signal of ZnO[22–25], whose origin is still debated[26]. However, it has been convincingly argued that this signal arises from ZnO nanostructures core-defect (CD), rather than from shell ones: it decreases and finally disappears by decreasing the nanoparticles size, from 500 nm to 5 nm of diameter[24]. This can explain why it is not present in our ZnO seed layer, made of a few nanoparticles aggregate, with a diameter lower than 50 nm. No shell-defect signal ($g \simeq 2$)[24,25] were observed, neither in the seed layer (too low amount of matter), nor in the NRs themselves (too large diameter).
The $g \simeq 1.96$ CD signal is fully resolved by lowering the static **B** field modulation from 5 to
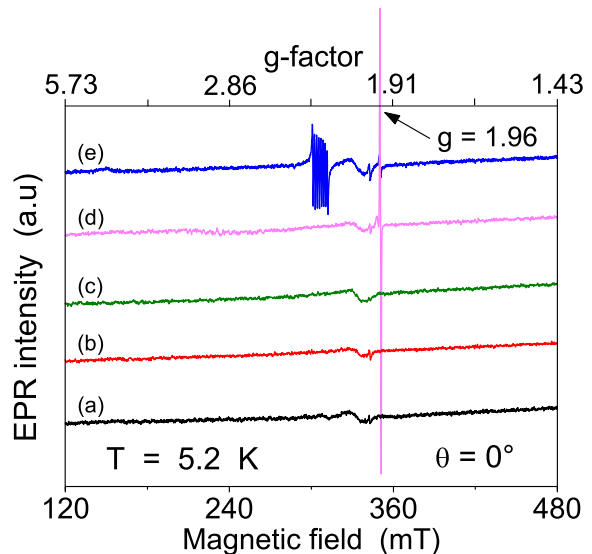

Figure 2: (color online) X-band EPR spectra (5 G modulation) at each steps of the nanorods fabrication. EPR sample holder (a), + sapphire substrate (b), + ZnO seed layer (c), + pure ZnO nanorods (d), + 5 % of Co in the synthesis solution (e). No baseline substraction or numerical smoothing.

1 G, then losing intensity in the same ratio, but letting a three-line structure appears (Fig. 3). The temperature-dependence study of these lines shows a uniform decrease of each ones intensity, displaying no levels populating/depopulating phenomena. This suggests the presence of three different and independant two-levels resonant centers, rather than a multi-levels one. However, we do not intend to discuss defect's nature debate, here we simply model the experimental data by a set of three independent 1/2 spin, with axially anisotropic g-factors: this is a mean of recording the experimental facts (relative transition intensities, line position and width), for later comparison or modeling. In doing so, a reasonable fit of the angle-dependent spectra (Fig. 3) is achieved with the parameters of table I. All simulations are made using the EasySpin MATLAB toolbox[27].

One of these defect's line is almost isotropic (D$_3$, $g_\parallel \simeq g_\perp$), while the other two display a slight axial anisotropy, consistently with the hexagonal wurtzite structure of the ZnO NRs. The observation of this anisotropy is a first evidence that the NRs are single crystalline and are mostly vertically oriented.

Regarding the modeling, it must be kept in mind that the slight observed anisotropy can not arise from true 1/2 spin (s electron), but rather from effective ones (ground states of p or d electrons, with spin-orbit). Then, the relative weight (I) for each simulation only gives the relative numbers
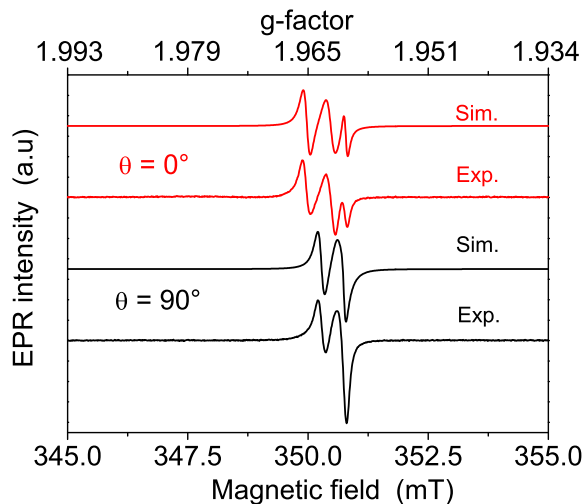
Figure 3: (color online) Experimental X-band EPR spectra (1 G modulation) of the $g \simeq 1.96$ signal for $B//z$ ($\theta = 0°$) and $B \perp z$ ($\theta = 90°$), recorded at $T = 5$ K. The shown simulations are performed with the parameters of Table I. The upper abscissa gives the corresponding g-factor value.

Table I: Label, spin, $\tilde{g}$-components, line width and intensities normalized to $I(D_1)$, for the three 1/2 spin models. Error bar for g-factor components is 2×10^{-4}.

Defect	spin	$g_\parallel$	$g_\perp$	w (mT)	I
D_1	1/2	1.9647	1.9630	0.26	1
D_2	1/2	1.9619	1.9607	0.36	1.63
D_3	1/2	1.9602	1.9604	0.15	0.23

of resonant centers if the transition probabilities are the same, which is not known. However, in section IV, taking into account the similarity of these three spin systems, we will assume 1/2 spin transition probability for each of them, and obtain an order of magnitude for their quantities.

We summarize the pure NRs study by noting that their EPR signals are well identified. They contain known ZnO CD and are mostly aligned perpendicularly to the substrate surface. No detectable traces of defects or impurities are observed, a fact which indicates relatively high purity of these samples.

B.   Cobalt-doped nanorods

When turning to the Co-doped NRs (S1 and S2 samples), two remarkable changes are visible in the EPR spectra (Fig. 2-e and Fig. 4): firstly, the CD signal ($g \sim 1.96$) intensity is lowered by a factor ~ 15, and, secondly, a Co-related signal appears at $g \sim 2.24$, for $\theta = 0°$, and at $g \sim 4.58$ for $\theta = 90°$.

The first point is an interesting indication that

a certain amount of incorporated Co is involved in the neutralization of the CDs, this is discussed in section IV. The three-lines structure of this signal has not been resolved for S1 and S2 samples, because of its very weak intensity.
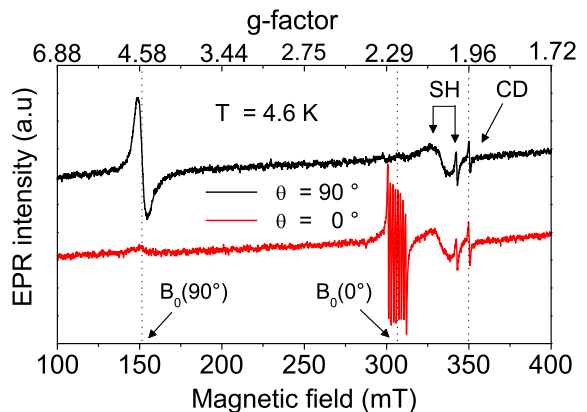

Figure 4: (color online) X-band EPR spectra of sample S2 for parallel ($\theta = 0°$) and perpendicular ($\theta = 90°$) orientation of $\mathbf{B}$ field. The CD and sample holder (SH) signals are indicated. Gravity centers of Co^{2+} signal for both orientation are shown.

Regarding the second point, the observed magnetic anisotropy of the Co^{2+} signal is a clear indication that the NRs are single crystalline and are well aligned, at least everywhere the Co ions give an EPR signal. Otherwise, the EPR spectra would tend to an isotropic powder spectra. For $\theta = 0°$, this Co-related signal displays an 8 lines structure (fully resolved in the spectra of Fig. 6), and a broad single line for $\theta = 90°$.

To make clear why these spectra are characteristic of Co^{2+} ions in easy-plane axial anisotropy, we present the levels diagram of such an ion in axial symmetry (Fig. 5). This diagram is a representation of the eigenvalues of the following single ion Hamiltonian, applied on $S = 3/2$ spin states:

$$H = D.S_z^2 + \mu_B \mathbf{S}.\tilde{\mathbf{g}}.\mathbf{B} + \mathbf{S}.\tilde{\mathbf{A}}.\mathbf{I} \qquad (1)$$

This spin Hamiltonian includes easy-plane axial anisotropy ($D > 0$), anisotropic Zeeman effect, and hyperfine coupling between the $S = 3/2$ electronic spin and the $I = 7/2$ nuclear one.

In bulk ZnO:Co, the situation is the following: first, below few Kelvins, the axial anisotropy ($D = 2.76$ cm^{-1}) constrains the 3/2 spin to stay in the hexagonal plane ($\pm 1/2$ projections). Then, the Zeeman term (depending on B and θ) polarizes the local moments along $\mathbf{B}$, by a splitting of the order of $h\nu$ (0.3 cm^{-1} for X-band EPR). The hyperfine coupling ($A_\parallel = 1.6 \times 10^{-3}$ cm^{-1}, $A_\perp = 0.3 \times 10^{-3}$ cm^{-1}) finally splits each Zeeman level into 8 levels, corresponding to the $(2I + 1)$ m_I projections.
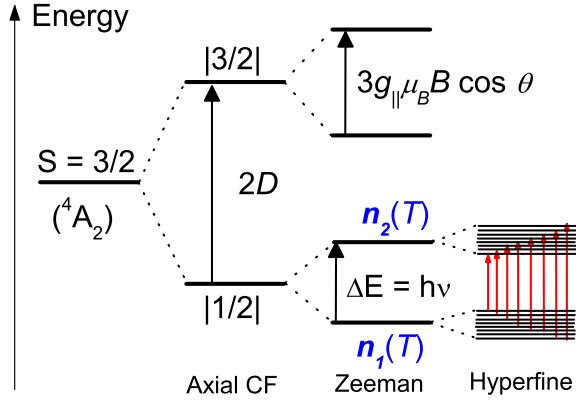
Figure 5: (color online) Levels diagram of an S=3/2 spin, under successive application of axial (easy-plane) anisotropy, Zeeman effect, and hyperfine interaction. Red arrows depict allowed EPR transitions between non-degenerate hyperfine levels.

The eight allowed EPR transitions ($\Delta m_S = \pm 1$, $\Delta m_I = 0$) are depicted in Fig. 5 by red arrows. At liquid helium temperature and above, the occupation number of the resonating levels is well approximated by n_1 and n_2. By solving the Zeeman interaction in the $\pm 1/2$ and $\pm 3/2$ subspaces separately, we obtain an expression for the ground state splitting:

$$\Delta E(B, \theta) = \mu_B B \sqrt{4 g_\perp^2 \sin^2 \theta + g_\parallel^2 \cos^2 \theta} \quad (2)$$

The above relation explains the observed anisotropy of the Co^{2+} signal gravity center B_0 (Fig. 4), which is defined by the relationship $\Delta E(B_0, \theta) = h\nu$. Then, for $\theta = 0°$, we have $h\nu = g_\parallel \mu_B B_0(0°)$, and for $\theta = 90°$, $h\nu = 2g_\perp \mu_B B_0(90°)$. As $g_\parallel \sim g_\perp$ (see Sec. IV), we obtain $B_0(90°) \simeq B_0(0°)/2$, which is experimentally observed in Fig. 4.
It is to be noted that at 5 K, the 3/2 spin are almost equally distributed between the $\pm 1/2$ and $\pm 3/2$ doublets, so that only half of them may contribute to the EPR signal. The excited $\pm 3/2$ doublet has no Zeeman splitting for $\theta = 90°$ (see Fig. 5), thus not contributing to the magnetization in this direction.

Regarding the NRs under study, the spectra of Fig. 4 allow us to determine $g_\parallel$ and $g_\perp$, which are found to be, respectively, 2.243 $\pm 10^{-3}$ and 2.270 $\pm 6 \times 10^{-3}$. These values are very close to the bulk values (2.243 and 2.279).
For $\theta = 90°$, the hyperfine structure is not resolved because the spacing between two hyperfine lines, $\Delta B = A_\perp / g_\perp \mu_B \simeq 0.3$ mT (with $A_\perp$ bulk value), is lower than the line width, which is of 0.6 mT for $\theta = 0°$ and larger for $\theta = 90°$. The $\theta = 0°$ orientation then brings more information, and is

the subject of the following discussion.
Fig. 6 shows the experimental spectra of samples S1 and S2, for $\theta = 0°$. Both have a line width of 0.6 mT and the same spacing between the hyperfine lines, $\Delta B = 1.54$ mT. This latter directly gives the parallel hyperfine coupling, $A_\parallel = \Delta B / g_\parallel \mu_B$, which is found to be 16×10^{-4} cm^{-1} in both samples, almost exactly equal to the bulk value[21].
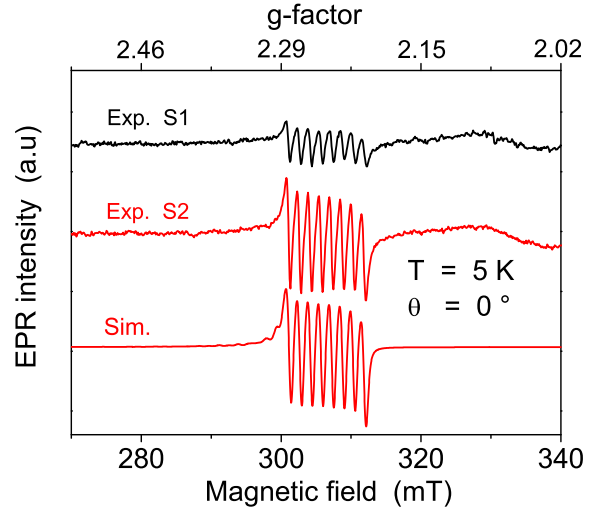

Figure 6: (color online) Experimental EPR spectra of S1 and S2 samples, recorded at 5 K and for $\theta = 0°$ orientation. The simulation of S2 spectra is made with parameters discussed in text.

Three of the five spin Hamiltonian parameters are thus directly deduced from the EPR spectra. Their closeness to the values for the bulk indicates that the local environment of Co^{2+} ions is very similar to that of the bulk case, so that we use bulk value for the two remaining ones (see Sec. IV). Realistic simulation with EasySpin[27] of the S2 spectra is obtained by introducing a Lorentzian distribution of the θ angle of 1.8° at half height, around $\theta = 0°$. This gives account for the observed intensity variation in the eight-line structure, and reflects the little misalignment of some of the NRs.

By comparing the S1 and S2 samples spectra, which differs by the Co amount in the synthesis solution (2 and 5 %, respectively), we observe that the Co^{2+} signal is well reproducible, with almost the same shape, and an intensity ratio of 2.7. Since the number of substitutional Co^{2+} ions is proportional to EPR intensity, it appears to scale with the synthesis solution Co concentration (ratio 2.5).

In order to quantify the number of substitutional Co^{2+} ions giving rise to the EPR signal, we have performed a temperature study of its intensity, and have compared it to the intensity of ZnO:Co TF of known Co^{2+} concentration (see Sec. II). The

EPR intensity is given by $I(T) = W.\Delta n(T).K$, where W is the transition probability, $\Delta n(T)$ is the temperature-dependent occupation number difference between the resonating levels, and K is a constant depending on experimental conditions (microwave power, modulation, etc.). Considering a set of independent (isolated) $S = 3/2$ spin described by the levels diagram of Fig. 5, Boltzmann statistic gives the occupation number of the two lowest levels, $n_1(T)$ and $n_2(T)$. By assuming $h\nu \ll kT$, the following expression for the relative difference $\Delta n/N = (n_1 - n_2)/N$ is derived:

$$\frac{\Delta n(T)}{N} \simeq \frac{h\nu}{2kT}\left(1 + e^{-\frac{2D}{kT}}\right)^{-1} \quad (3)$$

This modified Curie Law is a very good approximation for Δn above 1 K (see inset of Fig. 7). The temperature dependence of the Co^{2+} signal intensity can then be fitted by Eq. (3), with an adjustable prefactor including K, W and N. This has been done for the sample S2, which has the highest intensity, by a double integration of the EPR signal.

Doing the same for the TF reference sample, the fitting results in a different prefactor. As the transitions probabilities (W) and experimental conditions (K) are identical in both cases, the prefactors ratio gives the Co^{2+} number ratio, which is found to be $N_{TF}/N_{NR} = 430$. This is illustrated in Fig. 7, where the NRs Co^{2+} intensities have been reported, together with the best-obtained fit. In addition, the TF Co^{2+} intensities and their best fit, both divided by 430, are shown, so that the two fits are superimposed on each other.
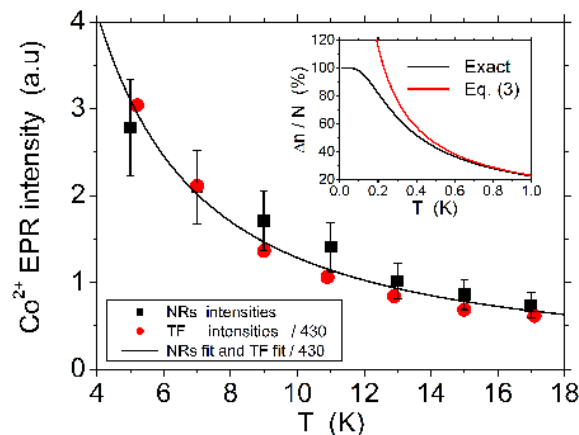

Figure 7: (color online) NRs and TF Co signal intensities as a function of temperature and best fit by Eq. (3). Errors on TF intensities ($\sim 5\%$) are not displayed for clarity. The inset shows the exact and approximated $\Delta n/N$ percentages at low temperature.

The ZnO:Co TF sample having a concentration of $x = 0.5$ % of Co^{2+} (see Sec. II), it contains

$N_{TF} = 2.5 \times 10^{15}$ of these ions. We then deduce that the number of substitutional Co^{2+} ion in the NRs of S2 sample is about 6×10^{12}. These absolute numbers of spin have to be seen as orders of magnitude because the double integration process results in large error bars: two baseline substractions have to be done, one before each integration. We estimate the error on NRs intensities to be of about 20 % (errors bars of Fig. 7), and that on TF intensities of about 5%. Then, from the intensity ratio between the EPR intensities of S1 and S2 samples (2.7), we find that S1 contains about 2×10^{12} substitutional Co^{2+} ions.

By assuming a uniform doping of the samples, we can estimate the mean concentration of the substitutional Co^{2+} in S1 and S2. Considering cylindrical NRs, we obtain the number of Zn sites they contain and, taking into account the NRs density in each samples, we deduce the following mean concentrations: $x(S1) \simeq 0.0002$ % and $x(S2) \simeq 0.0007$ %. These concentrations are very low, but are consistent with previous EPR study on ZnO:Co TF[18] where, due to the dipolar broadening, the hyperfine structure only begins to be resolved for $x < 0.1$ %.

IV.   DISCUSSION

The substitutional-Co^{2+} mean concentration in ZnO NRs deduced from the EPR study ($x(S1) \simeq 0.0002$ %, $x(S2) \simeq 0.0007$ %) allows us to make correspondence between the Co concentration in the synthesis solution, and the resulting mean Co^{2+} concentration in the NRs. This open the way to accurately estimate the cobalt concentration in such nano-DMS, and to study their properties.

In particular, it has been seen in section III B that the appearance of the substitutional Co^{2+} signal is accompanied by a large reduction of the CD signal. This indicates that some of the incorporated Co ions are involved in the CDs neutralization. However, this neutralization can be due to the substitutional Co^{2+} themselves, or to some other kind of incorporated Co (e.g interstitial[28,29]), not giving any EPR signal. This question is difficult to decide because we do not even know the exact nature of these CDs: multiple-levels defects, three different defects, or variations of the same defect. Moreover, the neutralization process is not necessarily a one-to-one process. It may require several Co ions to suppress one CD, or, in return, one Co ion may suppress several CDs. This suggest a possible interaction between intrinsic (CD) and extrinsic (Co^{2+}) defects within the ZnO matrix, as observed in ZnO:Mn mixed nanocrystals[30]. One interesting fact is that the

CD signal's intensity is the same in S1 and S2, thus indicating that a limit has been reached: adding more Co in the NRs will not suppress more CDs.

This result is consistent with previous study on Co-doped ZnO NRs grown at low temperature[31], which has stated that adding Co in the synthesis solution up to 1 % increases the bulk structural quality of the NRs, which is then degraded at higher concentration. This study has also shown that the actual resulting Co concentration within the NRs is significantly smaller than that of the synthesis solution, in accordance with our own findings.

On the other hand, we can attempt to quantify the CDs number in S0, S1, and S2 samples, and then to estimate the number of neutralized CDs. Assuming 1/2 spin transition probabilities for the CD EPR transitions, lines intensity of Co^{2+} and CD signals can be compared in order to give the ratio of their respective number. We find that S1 and S2 would contain approximately 1.5×10^{11} CDs, and S0 2.3×10^{12} of them. The number of neutralized defects would then be of about 2.2×10^{12}, which is of the order of the substitutional-Co^{2+} number in S1 and S2 (2×10^{12} and 6×10^{12}). However, this is not a proof that substitutional Co^{2+} ions are involved in the CDs neutralization, and a detailed EPR study with concentration on such NRs is then important to be performed, especially for lower concentration. It would be interesting to observe the progressive disappearance of the CD signal when introducing very low Co concentration, and to simultaneously check the optical and magnetic properties of the NRs. Such very low concentration of substitutional Co^{2+} would be difficult to detect because at $x(S1) \simeq 0.0002$ % the detection limit is practically reached, as seen in figure 6. Nevertheless, it is to be noted that at 5 K the $\Delta n/N$ ratio (proportional to EPR intensity) is only 4 % of its maximum. The inset of Fig. 7 shows that cooling down the sample to 1 K would give a ratio of 23 %, and that the maximum would be reached at 0.1 K. The detection of very low cobalt concentration then would require very low temperature, in order to increase EPR intensity.

Regarding the spin Hamiltonian parameters, three of five are found to be almost exactly similar to those of the bulk ZnO:Co, namely $g_\perp$, $g_\parallel$ and $A_\parallel$. The measurement of the others two (D and $A_\perp$) requires Q-band EPR, where $h\nu \simeq 1.2$ cm^{-1} (order of D). However, all these spin Hamiltonian parameters are not independent: they arise from the diagonalization in the 3d^7 space (Co^{2+} oxydation) of a larger Hamiltonian, which includes exact Coulomb repulsion within the 3d shell, spin-orbit interaction, and crystal-field components of even order. By treating the spin-orbit coupling and the axial part of crystal field as perturbation behind the Coulomb repulsion and the cubic part of the crystal field, the authors of Ref. 32 have obtained some analytical expressions for D, $g_\perp$, $g_\parallel$. Neglecting the influence of excited Coulomb multiplets in these expressions (Δ/B terms), we obtain the following relation:

$$D \simeq \frac{\xi_0}{6}\Delta g \qquad (4)$$

where ξ_0 is the free-ion spin-orbit coupling (570 cm^{-1}), and $\Delta g = g_\perp - g_\parallel$. The parameters D and Δg vary together, and are both zero for purely cubic crystal field. The measured Δg (0.027) leads to the value $D = 2.57$ cm^{-1}, which is close to the bulk one (2.76 cm^{-1}). It may reasonably be assumed that the same kind of relation is true for $\Delta A = A_\perp - A_\parallel$, so that we finally conclude that the spin Hamiltonian describing substitutional Co^{2+} ions in S1 and S2 has bulk parameters values.

The consequence is that the direct environment of Co^{2+} ions must be quite identical to that of bulk single crystal, in terms of lattice parameters, 3d wave-function extension, and hybridization with ligands.

The observed anisotropy indicates a high crystallinity of the NRs, but also a global coherent orientation of them, along the c-axis. It is to be noted that the NRs have all possible orientations *around* this c-axis but, this latter being sixfold degenerated, it does not give rise to any detectable magnetic anisotropy.

We then state that the NRs under study are highly crystalline and well-aligned, but have a too wide diameter (200-300 nm) for surface effects to arise. This is consistent with previous works on ZnO nanoparticles, in which nanosize effects appear for diameter lower than 50nm. An EPR study on Co-doped NRs with lower diameter deserved to be done in order to observed polarization surface effects, which would be signed by some substantial changes in spin Hamiltonian parameter, especially $g_\perp$ and $g_\parallel$. Higher values of these $\tilde{g}$-components would reflect a stronger magnetic anisotropy, which may affect other properties at higher temperature than few Kelvins.

Even without such changes in the anisotropy, the study of polarized-UV absorption at liquid helium temperature and with orientable applied magnetic field would be interesting to probe the magneto-optical coupling.

V. CONCLUSION

An EPR study of low-temperature (90°C) aqueous chemically grown vertically aligned, pure and

Co-doped, ZnO NRs have been performed at liquid helium temperature. The EPR spectra of pure and Co-doped samples indicate the high crystalline quality achieved by this synthesis route. The observed characteristic signal of Co^{2+} ions in easy-plane axial symmetry has proved the substitutional incorporation of Co in the ZnO matrix. These incorporated Co have been found to contribute to the neutralization of the nanocrystal's CDs. Comparison with a reference sample has allowed us to estimate the substitutional Co^{2+} concentration in the doped samples, and to relate it to the Co concentration in the synthesis solution. The presented results indicate the possibility of using the low-temperature aqueous chemical synthesis as a route to synthetize high crystalline quality DMS ZnO nanostructure with potential for developing spintronic based devices, like e.g ultra-fast spin dependent UV detectors.

VI. ACKNOWLEDGEMENT

[1] M. Willander, O. Nur, Q. X. Zhao, L. L. Yang, M. Lorenz, B. Q. Cao, J. Zúñiga Pérez, C. Czekalla, G. Zimmermann, M. Grundmann, A. Bakin, A. Behrends, M. Al-Suleiman, A. El-Shaer, A. Che Mofor, B. Postels, A. Waag, N. Boukos, A. Travlos, H. S. Kwack, J. Guinard, and D. Le Si Dang, Nanotechnology **20**, 332001 (2009).

[2] J.-H. Choi, H. Wang, S. J. Oh, T. Paik, P. S. Jo, J. Sung, X. Ye, T. Zhao, B. T. Diroll, C. B. Murray, and C. R. Kagan, *Science* **352**, 205 (2016).

[3] Y. Gu, I. L. Kuskovsky, M. Yin, S. O'Brien, and G. F. Neumark, Appl. Phys. Lett. **85**, 3833 (2004).

[4] Chey, C. O., Liu, X., Alnoor, H., Nur, O. and Willander, M. (2015), Phys. Status Solidi RRL, 9: 87−91.

[5] L. Sun, H. He, C. Liu, and Z. Ye, J. Appl. Phys. **108**, 124313 (2010)

[6] O. Lupan, T. Pauporte, L. Chow, G. Chai, B. Viana, V. V. Ursaki, E. Monaico, and I. M. Tiginyanu, Appl. Surf. Sci. **259**, 399 (2012).

[7] A. Echresh, C. O. Chey, M. Z. Shoushtari, O. Nur, and M. Willander, J. Appl. Phys. **116**, 193104 (2014).

[8] G. C. Park, S. M. Hwang, S. M. Lee, J. H. Choi, K. M. Song, H. Y. Kim, H.-S. Kim, S.-J. Eum, S.-B. Jung, J. H. Lim, and J. Joo, Sci. Rep. **5**, 10410 (2015).

[9] H. Alnoor, G. Pozina, V. Khranovskyy, X. Liu, D. Iandolo, M. Willander, and O. Nur, J. Appl. Phys. **119**, 165702 (2016).

[10] S. B. Orlinskii, J. Schmidt, P. G. Baranov, V. Lorrmann, I. Riedel, D. Rauh, and V. Dyakonov, Phys. Rev. B **77**, 115334 (2008).

[11] C. Y. Lin, W. H. Wang, C.-S. Lee, K. W. Sun, and Y. W. Suen, Appl. Phys. Lett. **94**, 151909 (2009).

[12] O. Lupan, T. Pauporte, B. Viana, V. V. Ursaki, I. M. Tiginyanu, V. Sontea, and L. Chow, J. Nanoelectron. Optoelectron. **7**, 712 (2012).

[13] P. R. Dorain, Phys. Rev. **112**, 1058 (1958).

[14] M. Diaconu, H. Schmidt, A. Pöppl, R. Böttcher, J. Hoentsch, A. Klunker, D. Spemann, H. Hochmuth, M. Lorenz, and M. Grundmann, Phys. Rev. B **72**, 085214 (2005).

[15] A. Savoyant, A. Stepanov, R. Kuzian, C. Deparis, C. Morhain, and K. Grasza, Phys. Rev. B **80**, 115203 (2009).

[16] T. Estle and M. de Wit, Bull. Am. Phys. Soc. **6**, 445 (1961).

[17] P. Sati, R. Hayn, R. Kuzian, S. Régnier, S. Schäfer, A. Stepanov, C. Morhain, C. Deparis, M. Laügt, M. Goiran, and Z. Golacki, Phys. Rev. Lett. **96**, 017203 (2006).

[18] P. Sati, A. Stepanov, and V. Pashchenko, Low Temp. Phys. **33**, 927 (2007).

[19] P. Sati, C. Deparis, C. Morhain, S. Schäfer, and A. Stepanov, Phys. Rev Lett. **98**, 137204 (2007)

[20] A. Ney, T. Kammermeier, K. Ollefs, S. Ye, V. Ney, T. C. Kaspar, S. A. Chambers, F. Wilhelm, and A. Rogalev, Phys. Rev. B **81**, 054420 (2010).

[21] A. Savoyant, F. Giovannelli, F. Delorme, and A. Stepanov, Semicond. Sci. Technol. **30** (2015) 075004.

[22] J. Schneider and A. Raüber, Z. Naturforsch. **16a**, 712 (1961).

[23] P. H. Kasai, Phys. Rev. **130**, 989 (1963).

[24] Jakes, P. and Erdem, E. (2011). Phys. Status Solidi RRL, 5: 56-58.

[25] H. Kaftelen, K. Ocakoglu, R. Thomann, S. Tu, S. Weber, and E. Erdem, Phys. Rev. B **86**, 014113 (2012).

[26] L. S. Vlasenko, Appl. Magn. Reson. (2010) 39:103-111.

[27] S. Stoll and A. Schweiger, J. Magn. Reson. **178**, 42 (2006)

[28] P. Lommens, F. Loncke, P. F. Smet, F. Callens, D. Poelman, H. Vrielinck, and Z. Hens, Chem. Mater., 2007, 19 (23), pp. 5576-5583.

[29] Lommens, P., Lambert, K., Loncke, F., De Muynck, D., Balkan, T., Vanhaecke, F., Vrielinck, H., Callens, F. and Hens, Z. (2008), ChemPhysChem, 9, 484−491.

[30] Ruf, T., Repp, S., Urban, J. et al. J Nanopart Res (2016) 18: 109.

[31] C.-W. Liu, S.-J. Chang, S. Brahma, C.-H. Hsiao, F. M. Chang, P. H. Wang, and K.-Y. Lo, J. Appl. Phys. **117**, 084315 (2015).

[32] R. O. Kuzian, A. M. Daré, P. Sati, and R. Hayn, Phys. Rev. B **74**, 155201 (2006).